Recombinant NAGLU-IGF2 prevents physical and neurological disease and improves survival in Sanfilippo B syndrome

Steven Q. Le,[1*] Shih-hsin Kan,[2*] Marie S. Roberts,[1] Joshua T. Dearborn,[1] Feng Wang,[3] Shan Li,[3] Elizabeth M. Snella,[4] Jackie K. Jens,[4] Bethann N. Valentine,[4] Hemanth R. Nelvagal,[1] Alexander Sorensen,[1] Keerthana Chintalapati,[1] Kevin Ohlemiller,[1] Carole Vogler,[5] Jonathan D. Cooper,[1] Tsui-Fen Chou,[3] N. Matthew Ellinwood,[4] Jodi D. Smith,[4] Mark S. Sands,[1] and Patricia I. Dickson[1**]

1. Washington University School of Medicine, St. Louis, Missouri, USA

2. CHOC Research Institute, Orange, California, USA

3. California Institute of Technology, Pasadena, California, USA

4. Iowa State University, Ames, Iowa, USA

5. Saint Louis University School of Medicine, St. Louis, Missouri, USA

*co-first authors

**Correspondence to:

Patricia I. Dickson, MD

4444 Forest Park Ave, Ste 5400

St. Louis, MO 63108

(314) 273-2943

pdickson@wustl.edu

Abstract

Recombinant human alpha-*N*-acetylglucosaminidase-insulin-like growth factor-2 (rhNAGLU-IGF2) is an investigational enzyme replacement therapy for Sanfilippo B, a lysosomal storage disease. Because recombinant human NAGLU (rhNAGLU) is poorly mannose 6-phosphorylated, we generated a fusion protein of NAGLU with IGF2 to permit its binding to the cation-independent mannose 6-phosphate receptor. We previously administered rhNAGLU-IGF2 intracerebroventricularly to Sanfilippo B mice, and demonstrated therapeutic restoration of NAGLU, normalization of lysosomal storage, and improvement in markers of neurodegeneration and inflammation. Here, we studied repeated intracerebroventricular rhNAGLU-IGF2 delivery in both murine and canine Sanfilippo B to determine potential effects on their behavioral phenotypes and survival. Treated mice showed improvement in disease markers such as heparan sulfate glycosaminoglycans, beta-hexosaminidase, microglial activation, and lysosomal-associated membrane protein-1. Sanfilippo B mice treated with rhNAGLU-IGF2 displayed partial normalization of their stretch attend postures, a defined fear pose in mice ($p<0.001$). We found an improved rotarod performance in Sanfilippo B mice treated with rhNAGLU-IGF2 compared to vehicle-treated Sanfilippo B mice ($p=0.002$). We also found a 61% increase in survival in Sanfilippo B mice treated with rhNAGLU-IGF2 (mean 53w, median 48w) compared to vehicle-treated Sanfilippo B mice (mean 33w, median 37w; $p<0.001$). In canine Sanfilippo B, we found that rhNAGLU-IGF2 administered into cerebrospinal fluid normalized HS and beta-hexosaminidase activity in gray and white matter brain regions. Proteomic analysis of cerebral cortex showed restoration of protein expression levels in pathways relevant to cognitive, synaptic, and lysosomal functions. These data suggest that treatment with rhNAGLU-IGF2 may improve the phenotype of Sanfilippo B disease.

Keywords: mucopolysaccharidosis, enzyme replacement therapy, glycosaminoglycan, proteomics, lysosomal storage disease

Introduction

Lysosomal storage diseases are a heterogenous group of inherited disorders characterized by accumulation of undegraded substrates within lysosomes. Typically, these disorders are caused by an inability to perform an enzymatic reaction, often due to deficiency in the production or function of a lysosomal hydrolase. Sanfilippo (types A-D) is collectively one of the most common lysosomal storage diseases, with incidence estimates ranging from 1 in 25,000 to 100,000.[1,2] Approximately fifteen percent of Sanfilippo disease is type B (*1*). The lysosomal storage material in Sanfilippo syndromes is the glycosaminoglycan heparan sulfate. The disease is associated with progressive neurodegeneration, typically with onset in early childhood (*2*). In the clinic, soluble lysosomal hydrolases are available in recombinant form for some types of lysosomal storage disease, and may be delivered by repeated infusion into the bloodstream or into the cerebrospinal fluid (*3-9*). However, no therapeutic options are currently approved for Sanfilippo syndrome.

To function as a therapeutic enzyme, a recombinant lysosomal hydrolase requires appropriate post-translational modification including glycosylation with mannose 6-phosphate (M6P) (*10*). Mannose 6-phosphate residues bind to mannose 6-phosphate receptors (M6PRs) expressed on the endosomal-lysosomal membrane, and results in transport of the enzyme from the Golgi apparatus to the lysosome, where it is active and catabolizes substrate in the acidic environment of this organelle. M6PRs are also present on the plasma membrane and mediate the endocytosis and subsequent trafficking of properly modified lysosomal enzymes from the extracellular milieu to the lysosome. One of the lysosomal hydrolases, the enzyme alpha-*N*-acetyl-glucosaminidase (NAGLU) that is responsible for Sanfilippo B syndrome (or mucopolysaccharidosis type IIIB, MPS IIIB), is not properly processed when produced recombinantly (*11, 12*). A fusion protein that contains the therapeutic enzyme (recombinant human NAGLU; rhNAGLU) plus a peptide fragment of IGF2, which can bind the cation-independent M6PR, forming rhNAGLU-IGF2 demonstrated improved intracellular uptake and reduction of lysosomal storage in Sanfilippo B fibroblasts (*13*). Using a mouse model, intracerebroventricular (ICV) delivery of rhNAGLU-IGF2 demonstrated therapeutic restoration of NAGLU, normalization of lysosomal storage, and dramatic improvement in markers of neurodegeneration and glial activation (*14*). Neonatal administration of rhNAGLU-IGF2 showed a treatment effect that lasted more than four weeks after a single ICV dose (*15*). A commercial form of rhNAGLU-IGF2 has reached clinical trials (*16-18*).

Recombinant enzymes delivered into cerebrospinal fluid can penetrate into deep brain structures and improve neuropathology in preclinical studies (*19-22*), and there is one recombinant therapeutic enzyme approved for intracerebroventricular administration in patients for the late-infantile form of neuronal ceroid lipofuscinosis (CLN2 disease) (*8*). Here, we studied the effect of intracerebroventricular rhNAGLU-IGF2 on behavior and survival in Sanfilippo B mice and studied effects upon biochemistry and proteomic profile of the brain of neonatal Sanfilippo B dogs.

Methods

Mouse model: *Naglu*-/- mice (B6.129S6-*Naglu*$^{tm1Efn/J}$, backbred onto the C57BL6/J strain for at least 10 generations) were produced by crossing -/- male mice with +/- female mice, thus generating approximately 50% affected progeny. Mice received research grade rhNAGLU-IGF2 (100 µg), rhNAGLU (100 µg), or an equivalent volume (~5 µl) of vehicle (artificial cerebrospinal fluid (CSF)) in the left lateral ventricle beginning at PND 2 by manual injection. At four weeks of age, mice were cannulated into the left ventricle, and the infusion of enzyme/vehicle was given via cannulae at 28-day intervals until 16 weeks of age. To prevent hypersensitivity reactions, mice received premedication with diphenhydramine 5 mg/kg intraperitoneally 15 min prior to infusions. Research grade rhNAGLU-IGF2, rhNAGLU, and vehicle were provided by BioMarin Pharmaceutical, Inc. (Novato, CA). Experimental personnel were blinded as to treatment of either therapeutic enzymes or vehicle (coded "1, 2 or 3"). All animal experiments were approved by the institutional animal use committees at the Los Angeles Biomedical Research Institute at Harbor-UCLA Medical Center (now the Lundquist Institute) in Torrance, CA, and Washington University School of Medicine in St. Louis, MO.

Auditory-evoked brainstem response (ABR) and electroretinography (ERG): ABR were performed as described (*23*) using Tucker-Davis Technologies System 3 Complete ABR/OAE Workstation equipped with a flashlamp system and Medusa RA16 preamplifier and headstage, and a Hewlett-Packard PC computer running SigGen and BioSig software (Tucker-Davis Technologies, Alachua FL). Stimuli at each frequency and level were presented 1,000 times at 20/sec. The minimum sound pressure level required for detection of a response was determined using a 5 dB minimum step size. Flash ERG was performed as described previously (*23-25*). Flash ERG measurements were recorded on a Tucker-Davis System 3 Complete ABR/OAE Workstation (Tucker-Davis Technologies, Alachua, FL, USA) and analyzed using BioSig software. Mice were dark-adapted for 2h to obtain a mixed rod/cone ERG, determined from the average response to 5–10 presentations of light at 0.1 Hz. Mice were light-adapted for 20 min to obtain a pure cone ERG, obtained by measuring the average response following 50 light flashes at a frequency of 1 Hz. Comparisons were made of the b-wave amplitudes in nanovolts from the best of three measurements of each of the light-adapted and dark-adapted responses.

Behavior: Male Sanfilippo B "mutant" mice and male carrier" mice were used for behavioral assessment at the UCLA Behavior Core. Elevated plus maze, novel object recognition, and social interaction tests were performed at the UCLA Behavioral Testing Core as previously described (*26*). The final infusion dose was given at 16 weeks of age, then infusion cannulae were removed before behavioral testing at 16-20 weeks of age was performed. Mice in these experiments were male and the implantation of cannulae prevented them from being caged with other males. To prevent confounding of behavioral experiments due to social isolation, these males were cohoused with a female companion and permitted to breed. This cohort of mice was euthanized at 20 weeks old following behavioral assessments.

Cohorts of mice of both sexes were studied at Washington University School of Medicine in St. Louis, Missouri. Activity in an open field was assessed at 22 weeks of age over 24 h in a rectangular polystyrene enclosure surrounded by photobeams monitored by computer software (MotorMonitor, Kinder Scientific, Poway, CA) (*27*). Testing consisted first of a 12 h block with the room lights off ("dark") and ended with a 12 h block with the room lights on ("light"). Mice had access to food and water *ad libitum* during testing. Outcome measures included number of

136 rearing events, distance traveled, and time spent resting. To test motor coordination (vestibular
137 and cerebellar function), animals were tested on a rotarod (UGO Basile, Verese, Italy) at 32 and
138 40 weeks as described (*23*). Briefly, a rocking paradigm with reversal of direction of rotation
139 after each full turn at 10 rpm for 3 minutes was executed for 3 consecutive days at 32 and 40
140 weeks of age. For each time point, training was provided for 2 consecutive days with 3 trials
141 each day and 20 minutes of rest between each trial. Testing occurred on the third consecutive day
142 and the length of time each mouse remained on the rod was recorded for all three trials and
143 averaged. The mice were euthanized at 40 weeks old following behavioral assessments.

144 **Survival:** In the survival experiment mutant mice were given monthly infusion starting at PND2
145 with vehicle (8 males, 8 females) or rhNAGLU-IGF2 (8 males, 8 females) as well as carrier mice
146 given vehicle (3 males, 13 females) or rhNAGLU-IGF2 (8 males, 8 females). The survival
147 experiment was carried to humane endpoints and terminated with the death of the last treated
148 mutant mice.

149 **Biochemical assays:** A subset of mice were used for biochemical analysis. Brains, liver, and
150 heart were removed. Spinal cords were removed by ejection. Tissues were frozen on dry ice and
151 stored at -80 °C until assay. NAGLU activity and total hexosaminidase activity were quantified
152 using 4-methylumbelliferyl assays as previously described (*15*). Briefly the enzymatic activity of
153 NAGLU and NAGLU–IGF2 was determined by hydrolysis of the fluorogenic substrate, 4-
154 methylumbelliferyl-*N*-acetyl-α-glucosaminide, obtained from CalBiochem (now EMD Millipore
155 Chemicals) or Toronto Research Chemicals, with minor modifications of a published protocol,
156 using 1.0 mM substrate in the incubation mixture (*28*). Enzymatic activity of beta-
157 hexosaminidase (combined A and B isoforms) was determined by hydrolysis of 4-
158 methylumbelliferyl-*N*-acetyl-β-glucosaminide (EMD Millipore Chemicals, Darmstadt, Germany)
159 using 1.25 mM substrate in the incubation mixture. For both enzymes, a unit of activity is
160 defined as release of 1 nmol of 4-methylumbelliferone (4MU) per hour. Protein concentration
161 was estimated by the Bradford method, using bovine serum albumin as a standard.

162 Analysis of heparan sulfate was performed by BioMarin Pharmaceutical (mouse tissues) or the
163 UC San Diego GlycoAnalytics Core (canine tissues) as described previously (*29*). Tissues were
164 homogenized and digested overnight with Pronase (Sigma-Aldrich, St. Louis, MO) in phosphate-
165 buffered at 37 °C and centrifuged at 14,000 rpm for 20 min. The supernatant was passed through
166 a DEAE column, and the bound GAG was eluted with 2 M NaCl. The GAG was then desalted on
167 PD10-size exclusion column, and purified GAG was lyophilized. Dried GAG disaccharides were
168 dissolved in aniline and reacted with freshly prepared sodium cyanoborohydride solution in a
169 dimethyl sulfoxide/acetic acid mixture (7:3, v/v). Reactions were carried out at 65 °C for 1 h
170 followed by 37 °C for 16 h. The samples were then dried using a speed vacuum at room
171 temperature. Aniline-tagged disaccharides were separated on a C18 column using an ion pairing
172 solvent mixture and analyzed by mass spectrometry in negative ion mode.

173 **Immunostaining:** Mice were anesthetized with isoflurane and perfused transcardially with
174 heparinized PBS followed by 4% paraformaldehyde in neutral PBS. After post-fixation in this
175 solution for an additional 48 hours, the brains were removed and cryoprotected in 30% sucrose in
176 50 mM tris buffered saline, pH=7.6. Spinal cords were divided into cervical, thoracic and
177 lumbosacral blocks, and 40µm coronal sections were cut throughout the cervical block on a
178 Thermofisher HM430 freezing microtome (Thermofisher). A one in six series of 40 µm coronal
179 brain sections from each mouse and a one in forty-eight series of spinal cord sections from each

mouse were stained on Superfrost Plus slides using a modified immunofluorescence protocol for the following antibodies: rat anti-mouse CD68, 1:400 (Bio-Rad, Hercules, CA, cat # MCA1957), rabbit anti-LAMP1, 1:400 (Abcam, Cambridge, MA, cat# Ab24170). The intensity of immunostaining was assessed using a semi-automated thresholding image analysis method, as described previously, using Image Pro-Premier software (MediaCybernetics, Chicago, IL) (*30*). Unbiased optical fractionator counts of the number of Nissl-stained ventral horn neurons from the cervical spine were obtained as described previously (*30, 31*), using StereoInvestigator software (Microbrightfield, MBF Bioscience, Williston, VT) and a design-based optical fractionator method. A one in forty-eight series of 40µm coronal spinal cord sections from each mouse were stained with cresyl fast violet (Brand, City). Cells were sampled with counting frames (70 × 40 µm) distributed over a sampling grid of 150 × 150 µm superimposed over the region of interest at 100 × magnification. Some vehicle-treated mutant and carrier control samples had undergone ex vivo imaging and were therefore not suitable for Nissl staining, so age-matched, untreated, mutant and carrier control mice were used.

Retinal histology: Eyes were obtained mice and immersion fixed in 2% glutaraldehyde/4% formaldehyde in PBS. Samples were embedded in Epon-Araldite resin and sectioned into 1-micron-thick sections and stained with toluidine blue as described (*23*). After careful alignment of orientation, the retinal thickness and the thickness of each layer were measured using ImageJ (*32*). Each measurement (e.g., length of outer nuclear layer, length of rods and cones layer, etc.) was performed in triplicate in ten locations along the axis of the eye for each mouse and the results averaged for each mouse.

Canine model: This work was performed in accordance with the *Guide for the Care and Use of Laboratory Animals* and approved by the Iowa State University institutional Animal Care and Use Committee (IACUC). Affected dogs were anesthetized and a 22-gauge needle inserted into the cisterna magna. CSF (0.2 to 0.5 ml) was collected free-flowing. A syringe was attached to the needle hub to deliver rhNAGLU-IGF2 at 1 week of age and again at 4 weeks of age (in sterile saline, total volume 300 µl at 1 week and 700 µl at 4 weeks). Dogs were euthanized at 8 weeks of age (4 weeks after the second dose). Dose was calculated per estimated brain weight. At one week of age, canine brains are roughly 1/38 of body weight, and the administered dose was 400 mg rhNAGLU-IGF2/kg brain, or approximately 7 mg. For a 2.5 kg four week-old pup, in which brain weight is 1/60 of body weight, the dose was approximately 17 mg. Control group animals were not treated. At necropsy, terminal CSF and blood were collected, and dogs were perfused with chilled PBS and brains removed. Brains were sliced coronally into 4 mm slabs using a pre-chilled, stainless steel canine brain matrix (ASI Instruments) as described elsewhere (*33*). A 3 mm biopsy punch was used to collect samples from cerebral gray matter, cerebral white matter, caudate, and cerebellar vermis. Samples were snap-frozen in an isopentane bath on dry ice.

Proteomics Snap-frozen canine samples (approximately 1x1x0.4 cm) from a parasagittal gyrus, including gray matter and subcortical white matter were analyzed by LC/MS/MS at Caltech. Protein lysates from canine brain cortex samples were prepared using Thermo EasyPrep Mini MS Sample Prep Kit (cat# A4006). Protein concentrations were determined using Bradford (Bio-Rad) and 100 µg total protein from each sample were prepared for mass spectrometry acquisition using Thermo EasyPep Mini MS Sample Prep Kit. After determining peptide concentrations by Pierce Quantitative Fluorometric Peptide Assay (cat# 23290), 20 µg peptide from each sample was labeled with TMT10plex Isobaric Label Reagent Set (ThermoFisher Scientific, cat# A37725) following to the manufacture's instruction. Labeled samples were combined and dried

using vacuum centrifugation. Samples were then separated into 8 fractions using the High pH reversed-phase peptide Fractionation Kit (ThermoFisher Scientific, cat# 84868). The fractions were dissolved with 0.1% formic acid and peptide concentration was determined with Quantitative Colorimetric Peptide Assay (ThermoFisher Scientific, cat# 23275).

TMT labeling LC-MS/MS experiments were performed using an EASY-nLC 1000 connected to an Orbitrap Eclipse Tribrid mass spectrometer (Thermo Scientific). 0.5 µg of each fraction was loaded onto an Aurora AUR2-25075C18A UHPLC Column (IonOpticks, Fitzroy, Australia) and separated over 131 min at a flow rate of 0.4 µL/min with the following gradient: 2-6% Solvent B (2 min), 6-22% B (78 min), 22-50% B (40 min), 50-95% B (1 min), and 95% B (10 min). Solvent A consisted of 97.8% H_2O, 2% ACN, and 0.2% formic acid, and solvent B consisted of 19.8% H_2O, 80% ACN, and 0.2% formic acid. An MS1 scan was acquired in the Orbitrap at 120k resolution with a scan range of 400-1600 m/z. The AGC target was 1×10^6, and the maximum injection time was 50 ms. Dynamic exclusion was set to exclude features after 1 time for 60 s with a 10-ppm mass tolerance. MS2 scans were acquired with CID activation type with the IonTrap. The isolation window was 0.7 m/z, the collision energy was 35%, the maximum injection time was 35 ms and the AGC target was 1×10^4. MS3 scans were acquired with HCD activation type in the Orbitrap at 60k resolution with a scan range of 100-500 m/z. The isolation window was 0.7 m/z, the collision energy was 65%, the maximum injection time was 118 ms and the AGC target was 2.5×10^5. Ion source settings were as follows: ion source type, NSI; spray voltage, 2300 V; ion transfer tube temperature, 300°C. System control and data collection were performed by Xcalibur software (ThermoFisher Scientific).

Data analysis: Graphs were produced on GraphPad Prism (version 9 or 9.1; GraphPad Software, San Diego, CA) or SigmaPlot version 14.0 (Systat Software Inc., San Jose, CA). Linear regression was performed using SigmaPlot. Statistical analysis of continuous variables was performed on Stata (version 16 or 17) or GraphPad Prism using ANOVA (if normal distribution), or if non-normal using Mann-Whitney. The proteomic data processing was performed through Proteome Discoverer 2.4 (ThermoFisher Scientific) using Uniprot canine database and the SequestHT with Percolator validation (*34, 35*). Normalization was performed relative to the total peptide amount. Further analyses were performed as below: limma analyses were performed using R studio following the user guide (*36*); volcano plot was generated with Origin 2019b; DE proteins were tested for enrichment analysis using g:Profiler (*37*) and plotted with Prism 7 (GraphPad Software, San Diego, CA); heatmaps were generated with Prism 7.

Results

Lysosomal storage: Male and female mice received ICV injections of rhNAGLU-IGF2, rhNAGLU, or vehicle at PND2. They were cannulated at 4 weeks of age and received therapeutic enzyme or vehicle via cannulae at monthly intervals until 16 weeks of age and euthanized 4 weeks later. Brain and heart showed a reduction in HS that reached statistical significance for each treatment group compared to vehicle-treated Sanfilippo B mice ($p<0.001$, **Fig. 1**). All intergroup differences were statistically significant by ANOVA. There was some residual NAGLU enzymatic activity detected in mouse brains in both treatment groups despite the 28-day interval from the final dose and tissue collection (**Supplemental Table S1**). Similar to previous studies, we found a reduction in the disease-associated marker beta-hexosaminidase in brain, liver, heart, and spinal cord of mice treated with rhNAGLU ($p=0.0016$) or rhNAGLU-IGF2 ($p<0.001$) compared to vehicle-treated Sanfilippo B mice (**Table 1**).

We also found decreased immunoreactivity for CD68, a marker of activated microglia, and LAMP1, a marker of lysosomes, in the primary somatosensory cortex (S1BF) and striatum (caudate and putamen) of mice treated with rhNAGLU or rhNAGLU-IGF2 (**Figs. 2 and 3**). Carrier mice treated with rhNAGLU or rhNAGLU-IGF2 did not differ from vehicle-treated carrier mice in LAMP1 or CD68 immunostaining in either brain region (not shown).

Spinal cord. Neuron counts of cervical spinal ventral horn were performed in a subset of mice. Sanfilippo B mice showed 18% lower mean estimated neuron counts compared to carrier controls ($p=0.021$, **Fig. 4**). Mice treated with rhNAGLU or rhNAGLU-IGF2 showed mean neuron counts that were not significantly different from carrier mice. The treated mice in both groups showed higher spinal neuron counts compared to untreated Sanfilippo B mice, and this reached statistical significance for mice treated with rhNAGLU ($p=0.014$) but not rhNAGLU-IGF2 ($p=0.088$).

Sanfilippo B mice showed increased CD68 staining compared to normal controls suggestive of activated microglia in cervical, thoracic, and lumbar gray matter of the spinal cord (**Supplemental Figure S1**). CD68 staining for activated macrophages in cervical spinal gray matter of Sanfilippo B mice showed consistent increases in the spinal cord dorsal and ventral horns compared to heterozygous normal mice or mice treated with rhNAGLU or rhNAGLU-IGF2 (**Fig. 5**). Similarly, LAMP1 immunostaining of the cervical spinal gray matter of Sanfilippo B mice showed increased staining qualitatively and quantitatively by threshold analysis of immunofluorescence signal in dorsal and ventral horns of the spinal cord compared to unaffected carrier mice (**Fig. 5**). Quantification of both markers in mice treated with rhNAGLU or rhNAGLU-IGF2 showed levels of immunostaining that were similar to those of unaffected carrier mice, with no significant differences in immunoreactivity between groups of mice treated with rhNAGLU and rhNAGLU-IGF2. Carrier mice treated with rhNAGLU or rhNAGLU-IGF2 did not differ from vehicle-treated carrier mice in LAMP1 or CD68 immunostaining (not shown).

Behavior: Male Sanfilippo B and control mice were treated with rhNAGLU, rhNAGLU-IGF2, or vehicle from PND2 to 16 weeks as described in the methods. We previously found that Sanfilippo B mice show reduced measures associated with fear in mice, as evidenced by decreased stretch attend postures on the elevated plus maze (*26*). This difference between normal

302 and Sanfilippo B mice was again seen here (**Fig. 4**), with a more normal number of stretch attend
303 postures in Sanfilippo B mice treated with either rhNAGLU or rhNAGLU-IGF2.

304 We did not find significant intergroup differences between vehicle-treated Sanfilippo B mice and
305 controls in radial arm maze performance, social interaction testing, dark/light activity, or novel
306 object recognition testing, such that these measures were not informative in assessing a
307 therapeutic response (**Supplemental Figures S2-S6**).

308 **Survival:** Sanfilippo B and control mice were treated with rhNAGLU-IGF2 or vehicle (four
309 groups; **Fig. 6**). The experiment was terminated after the last vehicle-treated mutant mouse died.
310 Results indicate a 58% increase in survival in Sanfilippo B mice treated with rhNAGLU-IGF2
311 (mean 52w, median 48w) compared to vehicle-treated Sanfilippo B mice (mean 33w, median
312 37w; $p<0.001$). Causes of death and other adverse events (mainly loss of cannulae and
313 reimplantation) are described in **Supplemental Table S3**.

314 **Motor Coordination:** Rotarod testing was performed in these mice at age 32 and 40 weeks, and
315 results are shown in **Fig. 7**. Sanfilippo B mice treated with vehicle showed slightly reduced
316 rotarod performance at 32 weeks ($p=0.0026$), with further worsening at 40 weeks ($p=0.004$).
317 Sanfilippo B mice treated with rhNAGLU-IGF2 showed improved rotarod performance
318 compared to vehicle-treated Sanfilippo B mice. Performance of the enzyme-treated mice was
319 similar to normal mice at age 32 weeks. At 40 weeks, treated mice performed significantly better
320 than vehicle-treated Sanfilippo B mice ($p=0.002$), but were also significantly different from
321 unaffected carrier controls ($p=0.006$). One Sanfilippo B mouse treated with vehicle and one
322 carrier mouse treated with rhNAGLU-IGF2 died between weeks 32 and 40.

323 **Hearing and vision**. Acoustic brainstem responses did not show intergroup differences between
324 Sanfilippo B mice and unaffected carrier mice (**Supplemental Figure S7**). Electroretinographs
325 showed retinopathy in Sanfilippo B mice that persisted despite treatment with rhNAGLU-IGF2
326 (**Fig. 8**). Cross-sectional analysis of the thickness of different layers of the retina post-mortem
327 showed reduced thickness in Sanfilippo B mice compared to carrier controls, which reached
328 statistical significance for the inner plexiform layer, outer nuclear layer, and rods and cones
329 (uncorrected p-values 0.040, 0.008, and 0.038, respectively). Mice treated with rhNAGLU-IGF2
330 showed increased thickness of the individual retinal layers, reaching statistical significance for
331 the outer nuclear layer (uncorrected p value 0.035).

332 **Canine studies:** This is naturally-occurring canine model of MPS IIIB, first identified in
333 Schipperke dogs, which provides advantages of a larger, more complex brain in which to test
334 therapeutic enzymes (*38, 39*). In this experiment, three Sanfilippo B dogs received two doses of
335 rhNAGLU-IGF2 (~7 mg at 1 week and ~17 mg at 4 weeks of age) into the cerebrospinal fluid at
336 the cisterna magna and were euthanized at 8 weeks of age, four weeks following the second and
337 final dose. Three untreated Sanfilippo B dogs and three untreated carrier dogs were used as
338 controls. Sanfilippo B dogs showed increased HS and beta-hexosaminidase levels in most brain
339 regions compared to controls (**Fig. 9**). These disease-associated changes were reduced essentially
340 to normal levels in treated animals, even in deeper regions of brain such as white matter and
341 caudate nucleus. Some NAGLU activity was detected in brain tissue despite a four-week interval
342 from the date of the final rhNAGLU-IGF2 dose and tissue collection (**Supplemental Table S3**).

343 Proteomic analysis was performed on cerebral cortical samples of each animal at the Chou lab as
344 described in the Methods (**Fig. 10**). Tandem mass tag (TMT) 10-plexed labelling was employed

345 to evaluate the proteomic changes in Sanfilippo B mutant animals. Specifically, we prepared
346 three independent biological wild type (CAR), Sanfilippo B (MUT) and rhNAGLU-IGF2-treated
347 Sanfilippo B (ERT) canine brain cortex samples. The TMT labeled samples were pooled and
348 further fractionated into 8 fractions and analyzed with the RTS-SPS-MS3 method(*40*). A total of
349 5806 proteins were identified, and 4442 of these proteins were quantified across all 9 samples
350 (**Supplemental Table S4**). We identified 309 proteins that demonstrated significantly different
351 quantities ($p < 0.05$) between the untreated Sanfilippo B (MUT) and wild type (CAR) samples
352 (**Supplemental Table S5**) by limma analysis. Among them, a set of 41 proteins with $\log_2$ (fold
353 change) >0.5 (up-regulated) or <-0.5 (down-regulated) was classified as the final differentially
354 expressed proteins (DEPs) (**Fig. 10A, Supplemental Table S6**). Subsequently, functional
355 enrichment analysis was performed on these 41 DEPs. The top four relevant changed cellular
356 components in the significantly enriched GO terms and top four changed KEGG or REAC
357 functional pathways are presented in **Fig. 10B**. The GO: CC analysis showed these DEPs were
358 mainly located at lysosome, secretory granule, extracellular matrix, and in vesicles. Pathway
359 analysis indicated the DEPs primarily related to Glycosaminoglycan degradation, Keratan sulfate
360 degradation, Neutrophil degranulation, and Innate Immune System. As shown in **Fig. 10C**, ERT
361 therapy reversed several proteins that were down-regulated in mutant animals compared to
362 carrier controls, such as DPP7 and CALB2. Notably, most of the elevated protein expression
363 seen in Sanfilippo B canines were reversed by ERT, including GNS, LAMP1, HEXB, and CD63,
364 among others. These results provide valuable insights for identifying novel hallmarks of
365 lysosomal diseases and therapeutic targets for Sanfilippo B.

366

367 **Discussion**

368 Early treatment of lysosomal disease is necessary for maximum therapeutic effect. Here,
369 we demonstrated that early treatment of Sanfililppo B mice and dogs with ICV enzyme
370 replacement therapy corrects biochemical abnormalities, neuropathology, behavior, and survival.
371 Our behavioral assessments were designed to separately evaluate the behaviors that might be
372 impacted by physical disease, such as motor activity and balance, from behaviors that are
373 primarily representative of altered central nervous system function, such as fear behavior. We
374 found evidence that rhNAGLU-IGF2 administration improved survival, physical disease, and
375 fear behavior in Sanfilippo B mice.

376 The IGF2 peptide was included to provide uptake of NAGLU via the IGF2-MPR,
377 because rhNAGLU (unlike naturally-occurring NAGLU) lacks mannose 6-phosphate. Uptake
378 and targeting via the MPR is an essential property of lysosomal enzymes. Neuronal cell lines
379 cultured *in vitro* rely on M6PRs for intracellular uptake, suggesting that treating these disease-
380 critical cells requires the use of this system (*15, 41, 42*). However, in this case we did not find a
381 therapeutic advantage to ICV rhNAGLU-IGF2 compared to rhNAGLU, although direct
382 comparison was limited in our study. A possible explanation for our findings is that the chosen
383 dose and/or frequency did not reveal differences between the efficacy of rhNAGLU and
384 rhNAGLU-IGF2 that might otherwise have been apparent. If the dose and frequency were higher
385 than necessary, nonspecific enzyme uptake would be expected to occur and possibly eliminate
386 the predicted differences between the native and fusion protein forms of enzyme. Alternatively,
387 if the dose were too low, microglial and perivascular cell uptake could have been predominant in
388 both the rhNAGLU and rhNAGLU-IGF2-treated groups. We previously demonstrated *in vivo* in
389 a murine model of Sly syndrome (mucopolysaccharidosis type VII) that glycosaminoglycan
390 levels and secondary enzyme elevations can be significantly reduced in the absence of any
391 demonstrable cellular enzyme uptake ((*43*). *In vitro* and *in vivo* studies of Sanfilippo B and other
392 lysosomal disorders have demonstrated that macrophage-lineage cells do not depend entirely on
393 M6PRs to engulf material from the extracellular milieu (*44, 45*), and this has also been observed
394 for mouse microglial cells incubated with rhNAGLU (*41*). In this scenario, both rhNAGLU and
395 rhNAGLU-IGF2 would have treated mainly these glial cells and not sufficiently treated the
396 neurons directly, resulting in a phenotypic improvement corresponding to correction in glial and
397 other supportive cells only. Even with enzymes that are well mannose 6-phosphorylated, such as
398 recombinant human alpha-L-iduronidase (for Hurler syndrome also known as MPS I) for
399 example, distribution studies of intravenously administered enzyme showed preferential
400 localization in sinusoidal cells with lesser staining appearing in hepatocytes. There could be a
401 "threshold effect" at work, in which saturating macrophage-lineage cells is necessary prior to
402 sufficient uptake into the target cells. It is not clear whether rhNAGLU or rhNAGLU-IGF2 were
403 taken up into neurons *in vivo* in the brain during the experiments described here, because we
404 were not able to assess biodistribution in our studies for the reasons described above. Previously
405 published studies of rhNAGLU-IGF2 did show staining for NAGLU in neurons (*14*), but the
406 dosing interval for that study was higher – four doses in two weeks – compared to the monthly
407 dosing used here. If monthly dose and frequency of administration of rhNAGLU-IGF2 was
408 inadequate to treat neurons yet sufficient to induce behavioral improvements, this implies that
409 our phenotypic read-outs in Sanfilippo B mice are not sufficient to measure the neurological
410 disease process and the impact of treatment upon this.

411

412 Besides enzyme replacement therapy, another approach in development is gene therapy
413 to deliver the coding sequence for *NAGLU* as a theoretically permanent means of correction.
414 Studies of adeno-associated viral vectors used to deliver NAGLU to Sanfilippo B mice show
415 improvements in HS, neuropathology, behavior, and survival that are similar to those reported
416 here for recombinant enzyme administration (*46, 47*). However, it is not known whether cells
417 that are transduced by viral vectors bearing the *NAGLU* transgene produce NAGLU that is
418 properly mannose 6-phosphorylated. Nevertheless, *in vitro* studies of NAGLU secreted by cells
419 transduced using adeno-associated viral vector-2 demonstrated that the secreted NAGLU was
420 able to correct intracellular HS accumulation as evidenced by an $^{35}SO_4$ assay (*48*). These authors
421 did not study competitive inhibition of this effect by mannose 6-phosphate (*49*), so it is not clear
422 whether the enzyme used that receptor system for uptake. It is likely that the concentration of
423 enzyme that is required for correction of glycosaminoglycan accumulation is far lower than that
424 required to demonstrate intracellular uptake of active enzyme (*50*). Both rhNAGLU-IGF2 and
425 rhNAGLU were capable of reducing intracellular HS in human Sanfilippo B fibroblasts *in vitro*,
426 although 10-fold higher concentrations of rhNAGLU compared to rhNAGLU-IGF2 were
427 required to achieve this effect (*41*). To study mannose 6-phosphorylation of NAGLU in the
428 context of gene therapy, induced pluripotent stem cells derived from Sanfilippo B mouse
429 embryonic fibroblasts were transduced with lentivirus bearing the human *NAGLU* transgene
430 under a cytomegalovirus promoter (*51*). The supernatant from these cells was added to
431 Sanfilippo B patient fibroblasts in the presence or absence of mannose 6-phosphate. The study
432 demonstrated uptake of NAGLU from the supernatant of these lentiviral-modified cells into
433 Sanfilippo B fibroblasts that was nearly completely abolished with the addition of mannose 6-
434 phosphate to the media, suggesting that NAGLU produced by gene therapy may not suffer the
435 same post-translational processing issues as recombinant NAGLU enzyme produced by cells *in*
436 *vitro,* as was used in this study.

437 In this study, as well as in our previous studies, enzyme replacement therapy
438 administered into the cerebral ventricle improved heparan sulfate and beta-hexosaminidase
439 activity levels in the liver and heart. The importance of treating disease outside of the brain in
440 Sanfilippo B syndrome is not known. Cardiac involvement is described in patients, including
441 valvular heart disease, myocardial thickening, and arrhythmia (*52, 53*). The disease course is
442 progressive, and while currently cardiac involvement is not a driver of mortality or even major
443 symptoms due to Sanfilippo B syndrome, it seems probable that if neurological disease is
444 successfully treated any morbidity from heart disease would become more evident.
445 Cerebrospinal fluid bulk turnover occurs multiple times per day (approximately three times per
446 day in humans), and so it is expected that recombinant enzymes administered into the
447 cerebrospinal fluid would reach the blood circulatory system, albeit at a lower concentration,
448 from which they would be taken up by organs and tissues outside the central nervous system. It
449 is not known whether this approach of delivering enzymes to the cerebrospinal fluid in order to
450 treat both the central nervous system and the rest of the body would be sufficient, holistic
451 therapy for lysosomal diseases that affect body as well as brain.

452 Canine proteomic analysis revealed altered expression of lysosomal proteins, such as
453 elevation of alpha-*N*-acetylglucosamine-6-sulfatase (GNS), cathepsin D (CTSD), and beta-
454 hexosaminidase (HEXB). These results are not surprising, as lysosomal enzymes and other
455 proteins may show elevated activity levels in tissues of Sanfilippo B mice compared to controls.
456 Marked deficiency in the protein dipeptidyl peptidase 7 (DPP7), has not to our knowledge been

457 previously associated with Sanfilippo B syndrome. Dipeptidyl peptidase 7 is a serine protease
458 that localizes to non-lysosomal vesicles and shows substrate specificity similar to that of the cell-
459 surface protein dipeptidyl peptidase 4 (*54*). Interestingly, HS and heparin oligosaccharides may
460 inhibit the activity of dipeptidyl peptidase 4 (*55*). Low expression of collagen type I alpha1
461 (COL1A1), collagen type I alpha2 (COL1A2), and fibulin 5 (FBLN5), proteins implicated in
462 connective tissue disorders, was found in Sanfilippo B dogs compared to controls, with more
463 normal expression in treated animals. Deficiency in collagen and fibulin is not known to be
464 associated with Sanfilippo B syndrome, but COL1A1 and COL1A2 have been described in the
465 glycosaminoglycan interactome (*56*).

466 Our study had a number of important limitations. First, the rhNAGLU-IGF2 that was
467 available for our studies was not materially the same as the candidate that is currently in clinical
468 trials. We do not know the differences in composition between the clinical candidate material
469 and the research grade enzyme that we used here. Second, our studies were not designed to
470 evaluate the biodistribution of either rhNAGLU or rhNAGLU-IGF2 in the central nervous
471 system. This is because our chosen study termination occurred four weeks after the final dose,
472 following behavioral studies. The half-life of rhNAGLU-IGF2 in the brain was previously
473 estimated at approximately seven days (*14*), although mice treated at postnatal day 1 or 2 showed
474 elevated NAGLU activity at four weeks following a single ICV injection of rhNAGLU-IGF2
475 (*15*). However, the dose of enzyme (100 µg) was not increased as the mice grew (*15*), so that in
476 this study little to no enzyme could be detected in the brain of these mice at four weeks after the
477 final infusion. This limitation also meant that we were unable to determine the cellular
478 distribution of the enzymes within tissues. Third, some behavioral assessments such as radial
479 arm maze and social interaction test did not show intergroup differences between carriers and
480 affected mice during this experiment, so that we could not use these tests to determine whether
481 there was a therapeutic effect in treated cohorts. All the mice were cannulated, which may have
482 affected their behavior and clearly limited the types of experiments we could conduct; for
483 example, we were not able to perform Morris water maze testing in cannulated mice. Both
484 control and treatment group experimental mice also underwent repeated sedation in order to dose
485 vehicle or enzyme, and it was important to keep treatment as consistent as possible among
486 groups. However, the repeated sedation events may have affected behavioral experiments and
487 impacted overall survival, even in the otherwise healthy carrier mice.

488

489 **Conclusions**:

490 Long-term treatment with monthly intracerebroventricular rhNAGLU-IGF2 (research grade)
491 showed a beneficial effect in Sanfilippo B mice. Significant intergroup differences were noted in
492 survival, motor activity, stretch attend postures (fear behavior), and histological markers of
493 microglial activation, and lysosomal substrate accumulation (HS, beta-hexosaminidase, LAMP1)
494 between enzyme-treated and vehicle-treated Sanfilippo B mice. Whole tissue brain and heart HS
495 levels were lower in Sanfilippo B mice treated with rhNAGLU compared to rhNAGLU-IGF2.
496 We did not detect other intergroup differences between rhNAGLU and rhNAGLU-IGF2-treated
497 mice in the outcome measures that we assessed in these experiments. Notably, our studies were
498 not designed to assess NAGLU distribution, and only one experiment included treatment groups
499 with both enzymes. Sanfilippo B dogs treated with rhNAGLU-IGF2 showed less HS in brain and
500 CSF compared to untreated affected controls, with beta-hexosaminidase activity normalized to

carrier levels in most cerebral areas including gray and white matter regions. Proteomics studies in cerebral cortex showed dysregulated pathways in Sanfilippo B dogs compared to carrier controls, with restoration of a more normal pattern in Sanfilippo B dogs treated with rhNAGLU-IGF2. These findings suggest that rhNAGLU-IGF2 administered into cerebrospinal fluid shows a beneficial effect on the Sanfilippo B phenotype in multiple species.

Acknowledgements:

P.I.D., J.T.D., M.S.S., and J.D.C. designed experiments and prepared the manuscript. S.Q.L., S.-h.K., M.S.R., and J.T.D. performed mouse experiments. S.Q.L, A.S., H.R.N., K.C., C.V. and J.D.C. performed histology including immunofluorescence and quantitative measurements. E.M.S., B.N.V., N.M.E., J.J., and J.D.S. performed canine experiments. F.W., S.L, S.Q.L., and T.F.C. performed enzyme assays and/or proteomics on canine tissues. We gratefully acknowledge the assistance and support of Soila Sukipolvi, Irina Zhuravka, George Lopez, Ling Wang, Valentina Sanguez, and Catalina Guerra. BioMarin Pharmaceutical and Allievex provided vehicle, rhNAGLU, and rhNAGLU-IGF2. BioMarin provided HS measurement of mouse brain and heart tissues. We gratefully acknowledge Roger Lawrence and Brett Crawford for their specific assistance with these assays.

Conflicts of Interest:

BioMarin Pharmaceutical Inc and Allievex provided research materials for this study. Dr. Dickson receives research support from Genzyme and research materials from M6P Therapeutics.

Funding:

Research was supported by R01 NS088766 to P.I.D and Lundquist Institute for Research Innovation at Harbor-UCLA Medical Center. The Washington University Animal Behavioral services are supported by the Eunice Kennedy Shriver National Institute Of Child Health & Human Development of the National Institutes of Health under Award Number P50 HD103525 to the Intellectual and Developmental Disabilities Research Center at Washington University. A traineeship from 5T32 GM8243-28 (to S.-h.K.) The content is solely the responsibility of the authors and does not necessarily represent the official views of the National Institutes of Health. The UCLA Behavioral Testing Core is supported by the UCLA Bioscience Core Funding Initiative. Immunofluorescence imaging was performed in part through the use of Washington University Center for Cellular Imaging (WUCCI) supported by Washington University School of Medicine, The Children's Discovery Institute of Washington University and St. Louis Children's Hospital (CDI-CORE-2015-505 and CDI-CORE-2019-813) and the Foundation for Barnes-Jewish Hospital (3770 and 4642).

536

537 **Table 1.** Beta-Hexosaminidase Activity in Mice (28 days post-dose)

	Brain 1+2	Brain 3	Brain 4	Brain 5+6	Spinal Cord	Liver	Heart
Mutant + Vehicle	3687 ± 244	3944 ± 280	3305 ± 112	2258 ± 276	2058 ± 273	3377 ± 907	1847 ± 296
Carrier + Vehicle	1318 ± 136	1420 ± 144	1307 ± 180	874 ± 220	746 ± 59.8	435 ± 35.6	190 ± 64.7
Mutant + NAGLU	1681 ± 173	1681 ± 67.6	1708 ± 106	955 ± 244	701 ± 74.3	755 ± 133	721 ± 335
Mutant + NAG-IGF2	2052 ± 265	1884 ± 321	1820 ± 320	1076 ± 258	706 ± 80.3	980 ± 307	858 ± 208

538 Values are means ± standard deviations and are expressed as units of activity per milligram
539 protein in homogenized tissue. Brains were divided coronally and numbered rostral to caudal 1-
540 6, with the 1st and 2nd combined and the 5th and 6th combined for the assay. NAG-IGF2:
541 rhNAGLU-IGF2, NAGLU: rhNAGLU. All values in the rhNAGLU or rhNAGLU-IGF2-treated
542 mutant mice were statistically significant compared with vehicle-treated mutant mice by Mann-
543 Whitney.

544

545 **Figure Legends**

546 Fig. 1. Heparan sulfate (HS) concentrations in the **(A)** brain and **(B)** heart of experimental mice
547 and controls. Mut: Sanfilippo B (*Naglu-/-*) mice. Car: heterozygous carrier (*Naglu +/-*) mice that
548 are expected to be phenotypically unaffected. NAG-IGF2: rhNAGLU-IGF2, NAGLU:
549 rhNAGLU. Mutant and Carrier control mice were treated with vehicle, and treatments and
550 vehicle were administered intracerebroventricularly as described in the methods. Units are
551 expressed in mg of wet weight, with means and standard deviation shown. N=8 per group.
552 Uncorrected p-value 0.0002 for Mut vs. Mut NAGLU or Mut NAG-IGF2 in both brain and heart
553 by Mann-Whitney.

554 Fig. 2. CD68 immunoreactivity in mouse brain. **(A-L)** Immunofluorescence staining with anti-
555 CD68 (green) in the primary somatosensory cortex (S1BF) and striatum (caudate and putamen)
556 in mice. Red boxes indicate insets for the panels below. Scalebar 100 µm in panels A-D and I-L.
557 Scalebar 500 µm in panels E-H. (**M-N**) Bar graphs depict means and standard deviations of
558 thresholding image analysis. N=4-9 per group. Uncorrected p-values show between-group
559 comparisons by Mann-Whitney**.** Mut (mutant): Sanfilippo B (*Naglu-/-*) mice. Car (carrier):
560 heterozygous (*Naglu +/-*) mice. NAGLU: rhNAGLU. NAG-IGF2: rhNAGLU-IGF2. Mutant
561 and Carrier control mice were treated with vehicle as described in the methods.

562 Fig. 3. LAMP1 immunoreactivity in mouse brain. **(A-H)** Immunofluorescence staining with anti-
563 LAMP1 (red) in the primary somatosensory cortex (S1BF) and striatum (caudate and putamen)
564 in mice. Scalebar 100 µm. **(I-J)** Bar graphs depict means and standard deviations of thresholding
565 image analysis. N=4-9 per group. Uncorrected p-values show between-group comparisons by
566 Mann-Whitney**.** Mut (mutant): Sanfilippo B (*Naglu-/-*) mice. Car (carrier): heterozygous (*Naglu*
567 *+/-*) mice. NAGLU: rhNAGLU. NAG-IGF2: rhNAGLU-IGF2. Mutant and Carrier control
568 mice were treated with vehicle as described in the methods.

569 Fig. 4. Neuron counts in mouse cervical spinal cord. Circles represent individual mice. Mut
570 (mutant): Sanfilippo B (*Naglu-/-*) mice. Car (carrier): heterozygous (*Naglu +/-*) mice. NAGLU:
571 rhNAGLU. NAG-IGF2: rhNAGLU-IGF2. Mutant and Carrier control mice were not treated
572 ("No Tx"). Unadjusted p-values show pairwise comparisons by ANOVA.

573 Fig. 5. CD68 and LAMP1 immunostaining in mouse cervical spinal cord. **A**) Representative
574 immunofluorescence images of axial sections of spinal cord stained for LAMP1 and CD68 (10x
575 magnification). **B**) Box plots showing median, first and third quartiles, and range of
576 immunoreactivity (IR) in dorsal (upper panels) and ventral (lower panels) cervical cord. Dots
577 represent individual mice. Mut (mutant): Sanfilippo B (*Naglu-/-*) mice. Car (carrier):
578 heterozygous (*Naglu +/-*) mice. NAGLU: rhNAGLU. NAG-IGF2: rhNAGLU-IGF2. Mutant
579 and Carrier control mice were treated with vehicle as described in the methods. *p=0.0022 and
580 **p=0.0095 vs. Mut by Mann-Whitney (uncorrected).

581 Fig. 6. Fear and Survival. A) Count of stretch attend postures during testing on the elevated plus
582 maze. Mut (mutant): Sanfilippo B (*Naglu-/-*) mice. Car (carrier): heterozygous (*Naglu +/-*) mice.
583 NAGLU: rhNAGLU. NAG-IGF2: rhNAGLU-IGF2. Mutant and Carrier control mice were
584 treated with vehicle as described in the methods. Carrier mice treated with rhNAGLU or
585 rhNAGLU-IGF2 did not differ from carrier mice treated with vehicle (not shown). Each symbol
586 = one mouse, with means and s.e.m. shown; N=7-14 per group. Numbers above brackets indicate
587 uncorrected p-values by Mann-Whitney. B) Survival curves for Sanfilippo B mice (Mut) and

588 carrier controls (Car) treated with ICV vehicle (Veh) or rhNAGLU-IGF2 (NAG-IGF2) monthly
589 from PND 2. N=16 per group, males and females. p<0.001 Mut-Veh versus Mut-NAG-IGF2.

590 Fig. 7. Time to fall off rotarod in Carrier ("Car," *Naglu*+/-) and Mutant ("Mut," *Naglu*-/-) mice
591 treated with vehicle or rhNAGLU-IGF2 (NAG-IGF2) ICV monthly from PND 2. Mice were
592 studied at (**A**) 32 and (**B**) 40 weeks. Mut – Vehicle, n=12 at 32 weeks and n=11 at 40 weeks;
593 Mut – NAG-IGF2, n=13; Car – vehicle, n=20; Carrier – NAG-IGF2, n=10 at 32 weeks and n=9
594 at 40 weeks. Dots show individual mice, boxes outline the median, 25th and 75th centile, and
595 whiskers depict range. Numbers above brackets indicate p-values by Mann-Whitney.

596 Fig. 8. Retinal disease in Sanfilippo B mice. **A)** Electroretinogram (ERG) in Sanfilippo B mice
597 treated with rhNAGLU-IGF2 (filled symbols) or carrier mice treated with vehicle (open
598 symbols). **B**) Retinal thickness by layer in Sanfilippo B mice treated with rhNAGLU-IGF2
599 (NAG-IGF2). IPL: inner plexiform layer; INL: inner nuclear layer; OPL: outer plexiform layer;
600 ONL: outer nuclear layer; R&C: rods and cones. Mutant: Sanfilippo B (*Naglu-/-*) mice. Carrier:
601 heterozygous (*Naglu* +/-) mice. NAG-IGF2: rhNAGLU-IGF2. Mutant and Carrier control mice
602 were treated with vehicle as described in the methods.

603 Fig. 9. Canine Sanfilippo B. Sanfilippo B dogs (MUT) and carrier controls (CAR) were treated
604 with intra-cisternal rhNAGLU-IGF2 (ERT) or untreated at 1 and 4 weeks of age and euthanized
605 at 8 weeks (n=3 per group, both sexes). **(A)** Box plot of heparan sulfate (HS) in left cerebral gray
606 matter (CGM). **(B)** Box plot of heparan sulfate (HS) in CSF. **(C)** Regression curve showing HS
607 in cerebrospinal fluid (CSF) versus HS in CGM. Open circles represent individual animals. (D)
608 Beta-hexosaminidase in brain regions (means and standard deviation). CSO: centrum semiovale.
609 CN: caudate nucleus. CGM: cerebral gray matter. CWM: cerebral white matter.

610 Fig. 10. Proteomic analysis in canine Sanfilippo B. Experimental animals were the same as in
611 Fig. 9 and included heterozygous carriers (CAR), Sanfilippo B (MUT), and rhNAGLU-IGF2-
612 treated Sanfilippo B (ERT) groups. Proteins were analyzed from canine brain cortex. **(A)**
613 Volcano plot displaying the proteomic changes in Sanfilippo B mutant, n=3. **(B)** Functional
614 enrichment analysis of the differently expressed proteins affected by Sanfilippo B mutant. **(C)**
615 Heatmap displaying the scaled abundance of the differently expressed proteins affected by
616 Sanfilippo B mutant and rhNAGLU-IGF2 treatment.

617 **References**

618

619 1. B. Héron *et al.*, Incidence and natural history of mucopolysaccharidosis type III in France
620 and comparison with United Kingdom and Greece. *American Journal of Medical*
621 *Genetics, Part A* **155A**, 58-68 (2011).
622 2. M. Valstar, G. Ruijter, O. van Diggelen, B. Poorthuis, F. Wijburg, Sanfilippo syndrome:
623 A mini-review. *Journal of Inherited Metabolic Disease* **31**, 240-252 (2008).
624 3. E. D. Kakkis *et al.*, Enzyme-replacement therapy in mucopolysaccharisosis I. *New*
625 *England Journal of Medicine* **344**, 182-188 (2001).
626 4. P. S. Kishnani *et al.*, Recombinant human acid alpha-glucosidase: Major clinical benefits
627 in infantile-onset Pompe disease. *Neurology* **68**, 99-109 (2007).
628 5. P. Harmatz *et al.*, Pharmacokinetic profile of recombinant human N-acetylgalactosamine
629 4-sulphatase enzyme replacement therapy in patients with mucopolysaccharidosis VI
630 (Maroteaux-Lamy syndrome): a phase I/II study. *Acta Paediatrica Suppl* **94**, 61-68
631 (2005).
632 6. C. M. Eng *et al.*, Safety and efficacy of recombinant human alpha-galactosidase A
633 replacement therapy in Fabry's disease. *N. Engl. J. Med.* **345**, 9-16 (2001).
634 7. N. J. Weinreb *et al.*, Effectiveness of enzyme replacement therapy in 1028 patients with
635 type 1 Gaucher disease after 2 to 5 years of treatment: a report from the Gaucher
636 Registry. *The American Journal of Medicine* **113**, 112-119 (2002).
637 8. A. Schulz *et al.*, Study of Intraventricular Cerliponase Alfa for CLN2 Disease. *New*
638 *England Journal of Medicine* **378**, 1898-1907 (2018).
639 9. J. Cadaoas *et al.*, Vestronidase alfa: Recombinant human β-glucuronidase as an enzyme
640 replacement therapy for MPS VII. *Molecular Genetics and Metabolism* **130**, 65-76
641 (2020).
642 10. S. Hickman, L. J. Shapiro, E. F. Neufeld, A recognition marker required for uptake of a
643 lysosomal enzyme by cultured fibroblasts. *Biochemical and Biophysical Research*
644 *Communications* **57**, 55-61 (1974).
645 11. K. W. Zhao, E. F. Neufeld, Purification and characterization of recombinant human
646 alpha-N-acetylglucosaminidase secreted by Chinese hamster ovary cells. *Protein*
647 *expression and purification* **19**, 202-211 (2000).
648 12. B. Weber, J. J. Hopwood, G. Yogalingam, Expression and characterization of human
649 recombinant and alpha-N-acetylglucosaminidase. *Protein expression and purification* **21**,
650 251-259 (2001).
651 13. S.-H. Kan *et al.*, Insulin-like growth factor II peptide fusion enables uptake and
652 lysosomal delivery of α-N-acetylglucosaminidase to mucopolysaccharidosis type IIIB
653 fibroblasts. *Biochemical Journal* **458**, (2014).
654 14. S.-h. Kan *et al.*, Delivery of an enzyme-IGFII fusion protein to the mouse brain is
655 therapeutic for mucopolysaccharidosis type IIIB. *Proceedings of the National Academy*
656 *of Sciences USA* **111**, 14870-14875 (2014).
657 15. S. h. Kan *et al.*, Biochemical evaluation of intracerebroventricular rhNAGLU-IGF2
658 enzyme replacement therapy in neonatal mice with Sanfilippo B syndrome. *Molecular*
659 *Genetics and Metabolism* **133**, 185-192 (2021).
660 16. M. Aoyagi-Scharber *et al.*, Clearance of Heparan Sulfate and Attenuation of CNS
661 Pathology by Intracerebroventricular BMN 250 in Sanfilippo Type B Mice. *Molecular*
662 *Therapy - Methods & Clinical Development* **6**, 43-53 (2017).

663 17. A. Grover *et al.*, Translational studies of intravenous and intracerebroventricular routes of
664 administration for CNS cellular biodistribution for BMN 250, an enzyme replacement
665 therapy for the treatment of Sanfilippo type B. *Drug Delivery and Translational*
666 *Research* **10**, 425-439 (2020).
667 18. N. Muschol *et al.*, A phase I/II study on intracerebroventricular tralesinidase alfa in
668 patients with Sanfilippo syndrome type B. *J Clin Invest* **133**, (2023).
669 19. P. V. Belichenko *et al.*, Penetration, diffusion, and uptake of recombinant human alpha-
670 L-iduronidase after intraventricular injection into the rat brain. *Molecular Genetics and*
671 *Metabolism* **86**, 141-149 (2005).
672 20. P. Dickson *et al.*, Intrathecal enzyme replacement therapy: successful treatment of brain
673 disease via the cerebrospinal fluid. *Mol Genet Metab.* **91**, 61-68 (2007).
674 21. A. Chen *et al.*, Glycosaminoglycan storage in neuroanatomical regions of
675 mucopolysaccharidosis I dogs following intrathecal recombinant human iduronidase.
676 *APMIS* **119**, 513-521 (2011).
677 22. C. H. Vite *et al.*, Features of brain MRI in dogs with treated and untreated
678 mucopolysaccharidosis type I. *Comparative medicine* **63**, 163-173 (2013).
679 23. C. D. Heldermon *et al.*, Development of sensory, motor and behavioral deficits in the
680 murine model of Sanfilippo syndrome type B. *PloS one* **2**, e772 (2007).
681 24. K. K. Ohlemiller, C. A. Vogler, M. Roberts, N. Galvin, M. S. Sands, Retinal function is
682 improved in a murine model of a lysosomal storage disease following Bone Marrow
683 transplantation. *Experimental Eye Research* **71**, 469-481 (2000).
684 25. A. K. Hennig *et al.*, AAV-Mediated Intravitreal Gene Therapy Reduces Lysosomal
685 Storage in the Retinal Pigmented Epithelium and Improves Retinal Function in Adult
686 MPS VII Mice. *Mol Ther* **10**, 106-116 (2004).
687 26. S.-h. Kan *et al.*, Behavioral deficits and cholinergic pathway abnormalities in male
688 Sanfilippo B mice. *Behavioural Brain Research* **312**, 265-271 (2016).
689 27. J. T. Dearborn *et al.*, Comprehensive functional characterization of murine infantile
690 Batten disease including Parkinson-like behavior and dopaminergic markers. *Scientific*
691 *Reports* **5**, 1-16 (2015).
692 28. J. Marsh, A. H. Fensom, 4-methylumbelliferyl α-N-acetylglucosaminidase activity for
693 diagnosis of Sanfilippo B disease. *Clinical Genetics* **27**, 258-262 (2008).
694 29. R. Lawrence *et al.*, Disease-specific non-reducing end carbohydrate biomarkers for
695 mucopolysaccharidoses. *Nat Chem Biol* **8**, 197-204 (2012).
696 30. H. R. Nelvagal, J. T. Dearborn, J. R. Ostergaard, M. S. Sands, J. D. Cooper, Spinal
697 manifestations of CLN1 disease start during the early postnatal period. *Neuropathology*
698 *and Applied Neurobiology* **47**, 251-267 (2021).
699 31. C. Kielar *et al.*, Successive neuron loss in the thalamus and cortex in a mouse model of
700 infantile neuronal ceroid lipofuscinosis. *Neurobiology of Disease* **25**, 150-162 (2007).
701 32. P. Lotfi *et al.*, Trehalose reduces retinal degeneration, neuroinflammation and storage
702 burden caused by a lysosomal hydrolase deficiency. *Autophagy* **14**, 1419-1434 (2018).
703 33. M. T. Egeland *et al.*, Central nervous system pathology in preclinical MPS IIIB dogs
704 reveals progressive changes in clinically relevant brain regions. *Scientific Reports* **10**,
705 20365 (2020).
706 34. J. K. Eng, A. L. McCormack, J. R. Yates, An approach to correlate tandem mass spectral
707 data of peptides with amino acid sequences in a protein database. *Journal of the*
708 *American Society for Mass Spectrometry* **5**, 976-989 (1994).

709 35. M. Spivak, J. Weston, L. Bottou, L. Käll, W. S. Noble, Improvements to the percolator
710 algorithm for peptide identification from shotgun proteomics data sets. *Journal of*
711 *Proteome Research* **8**, 3737-3745 (2009).
712 36. G. K. Smyth, N. Thorne, J. Wettenhall, Limma: Linear Models for Microarray Data
713 User's Guide. 2003.
714 37. U. Raudvere *et al.*, G:Profiler: A web server for functional enrichment analysis and
715 conversions of gene lists (2019 update). *Nucleic Acids Research* **47**, W191-W198 (2019).
716 38. N. M. Ellinwood *et al.*, A model of mucopolysaccharidosis IIIB (Sanfilippo syndrome
717 type IIIB): N-acetyl-alpha-D-glucosaminidase deficiency in Schipperke dogs. *J. Inherit.*
718 *Metab. Dis.* **26**, 489-504 (2003).
719 39. K. Raj, N. M. Ellinwood, U. Giger, An exonic insertion in the NAGLU gene causing
720 Mucopolysaccharidosis IIIB in Schipperke dogs. *Sci Rep* **10**, 3170 (2020).
721 40. D. K. Schweppe *et al.*, Full-Featured, Real-Time Database Searching Platform Enables
722 Fast and Accurate Multiplexed Quantitative Proteomics. *Journal of Proteome Research*
723 **19**, 2026-2034 (2020).
724 41. G. Yogalingam *et al.*, BMN 250, a fusion of lysosomal alpha-N-acetylglucosaminidase
725 with IGF2, exhibits different patterns of cellular uptake into critical cell types of
726 Sanfilippo syndrome B disease pathogenesis. *PLOS ONE* **14**, e0207836 (2019).
727 42. H. Prill *et al.*, Differential Uptake of NAGLU-IGF2 and Unmodified NAGLU in Cellular
728 Models of Sanfilippo Syndrome Type B. *Molecular Therapy - Methods and Clinical*
729 *Development* **14**, 56-63 (2019).
730 43. A. Donsante, B. Levy, C. Vogler, M. S. Sands, Clinical response to persistent, low-level
731 beta-glucuronidase expression in the murine model of mucopolysaccharidosis type VII. *J*
732 *Inherit Metab Dis* **30**, 227-238 (2007).
733 44. M. S. Sands *et al.*, Biodistribution, Kinetics, and Efficacy of Highly Phosphorylated and
734 Non-phosphorylated Beta-Glucuronidase in the Murine Model of Mucopolysaccharidosis
735 VII. *Journal of Biological Chemistry* **276**, 43160-43165 (2001).
736 45. S. Q. Le *et al.*, A Humoral Immune Response Alters the Distribution of Enzyme
737 Replacement Therapy in Murine Mucopolysaccharidosis Type I. *Molecular Therapy -*
738 *Methods & Clinical Development* **8**, 42-51 (2018).
739 46. H. Fu, A. S. Meadows, T. Ware, R. P. Mohney, D. M. McCarty, Near-Complete
740 Correction of Profound Metabolomic Impairments Corresponding to Functional Benefit
741 in MPS IIIB Mice after IV rAAV9-hNAGLU Gene Delivery. *Molecular Therapy* **25**,
742 792-802 (2017).
743 47. H. Fu *et al.*, Significantly increased lifespan and improved behavioral performances by
744 rAAV gene delivery in adult mucopolysaccharidosis IIIB mice. *Gene Ther.* **14**, 1065-
745 1077 (2007).
746 48. H. Fu *et al.*, Neurological correction of lysosomal storage in a mucopolysaccharidosis
747 IIIB mouse model by adeno-associated virus-mediated gene delivery. *Molecular Therapy*
748 **5**, 42-49 (2002).
749 49. J. DiRosario *et al.*, Innate and adaptive immune activation in the brain of MPS IIIB
750 mouse model. *Journal of Neuroscience Research* **87**, 978-990 (2009).
751 50. E. D. Kakkis, A. Matynia, A. J. Jonas, N. E. F, Overexpression of the human lysosomal
752 enzyme á-l-iduronidase in Chinese hamster ovary cells. *Prot. Expr. Purif.* **5**, 225-232
753 (1994).

754 51. D. Clarke *et al.*, Genetically Corrected iPSC-Derived Neural Stem Cell Grafts Deliver
755 Enzyme Replacement to Affect CNS Disease in Sanfilippo B Mice. *Molecular Therapy -*
756 *Methods and Clinical Development* **10**, 113-127 (2018).
757 52. H. Y. Lin *et al.*, Cardiac characteristics and natural progression in Taiwanese patients
758 with mucopolysaccharidosis III. *Orphanet Journal of Rare Diseases* **14**, 140 (2019).
759 53. S. C. M. Nijmeijer, R. H. A. C. M. de Bruin-Bon, F. A. Wijburg, I. M. Kuipers, Cardiac
760 disease in mucopolysaccharidosis type III. *Journal of Inherited Metabolic Disease* **42**,
761 276-285 (2019).
762 54. M. Chiravuri, F. Agarraberes, S. L. Mathieu, H. Lee, B. T. Huber, Vesicular Localization
763 and Characterization of a Novel Post-Proline-Cleaving Aminodipeptidase, Quiescent Cell
764 Proline Dipeptidase. *The Journal of Immunology* **165**, 5695-5702 (2000).
765 55. R. Sadir, A. Imberty, F. Baleux, H. Lortat-Jacob, Heparan sulfate/heparin
766 oligosaccharides protect stromal cell-derived factor-1 (SDF-1)/CXCL12 against
767 proteolysis induced by CD26/dipeptidyl peptidase IV. *Journal of Biological Chemistry*
768 **279**, 43854-43860 (2004).
769 56. S. D. Vallet, C. Berthollier, S. Ricard-Blum, The glycosaminoglycan interactome 2.0. *Am*
770 *J Physiol Cell Physiol* **322**, C1271-C1278 (2022).

771

772 Figure 1

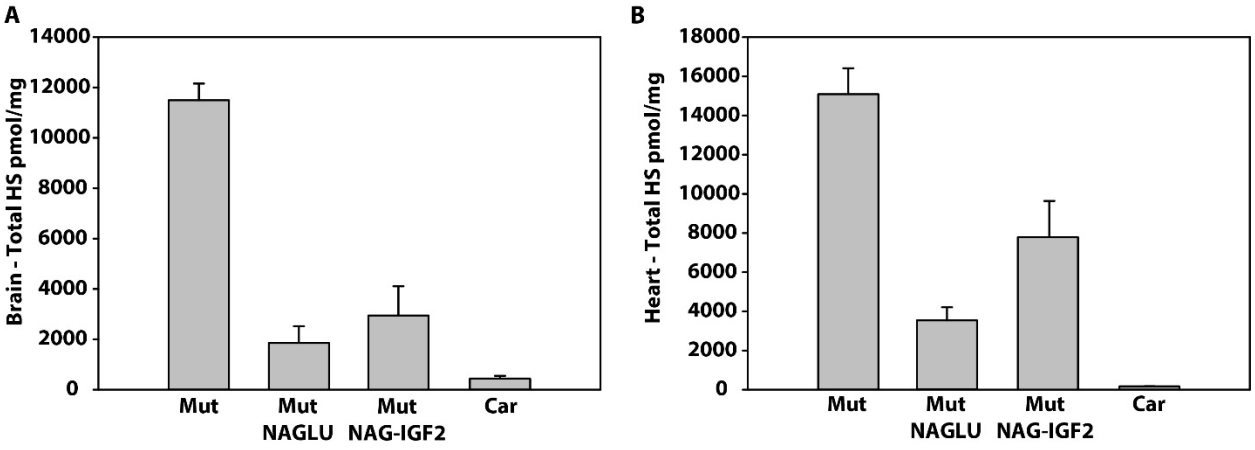

773

774 Figure 2

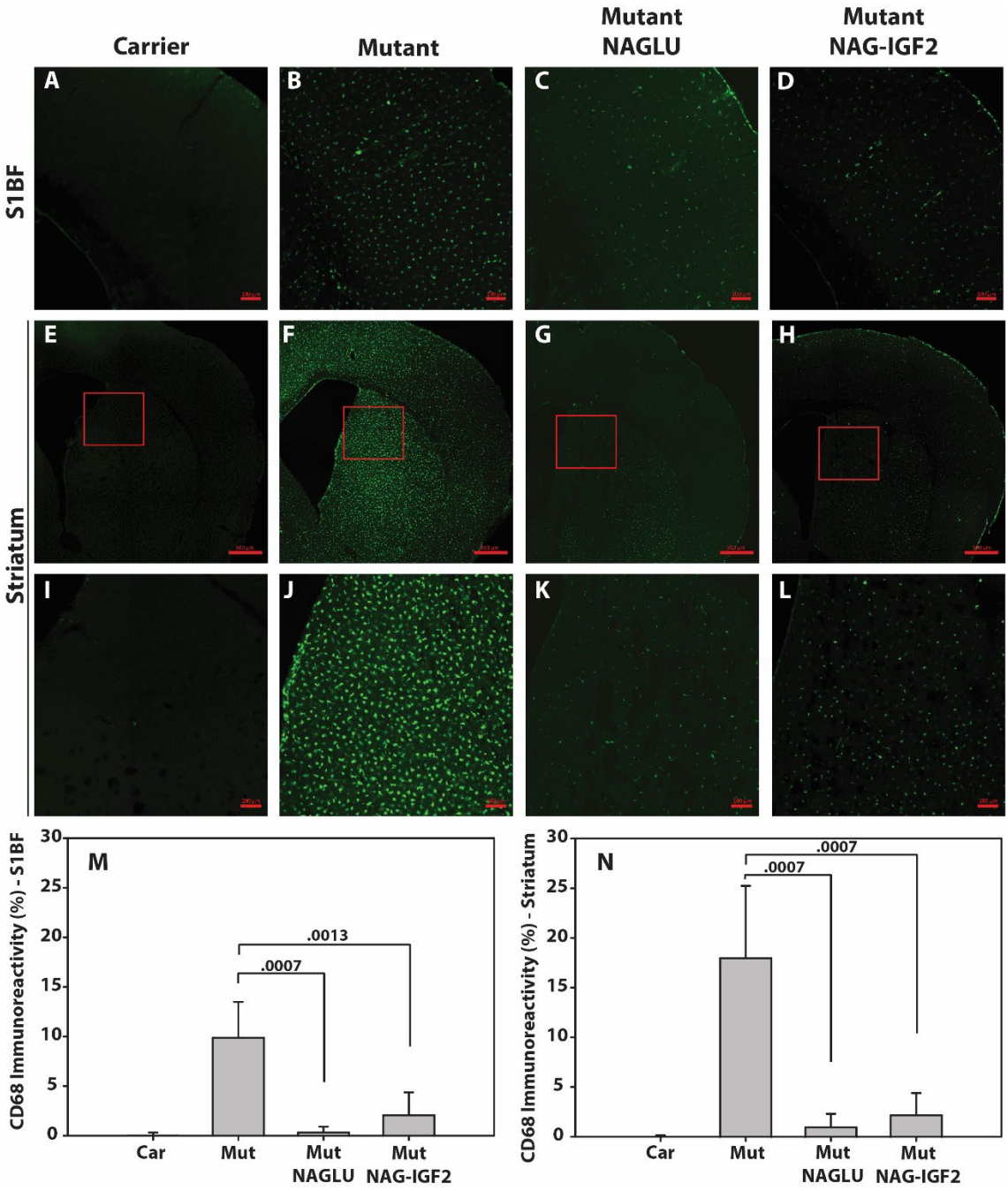

775

776 Figure 3

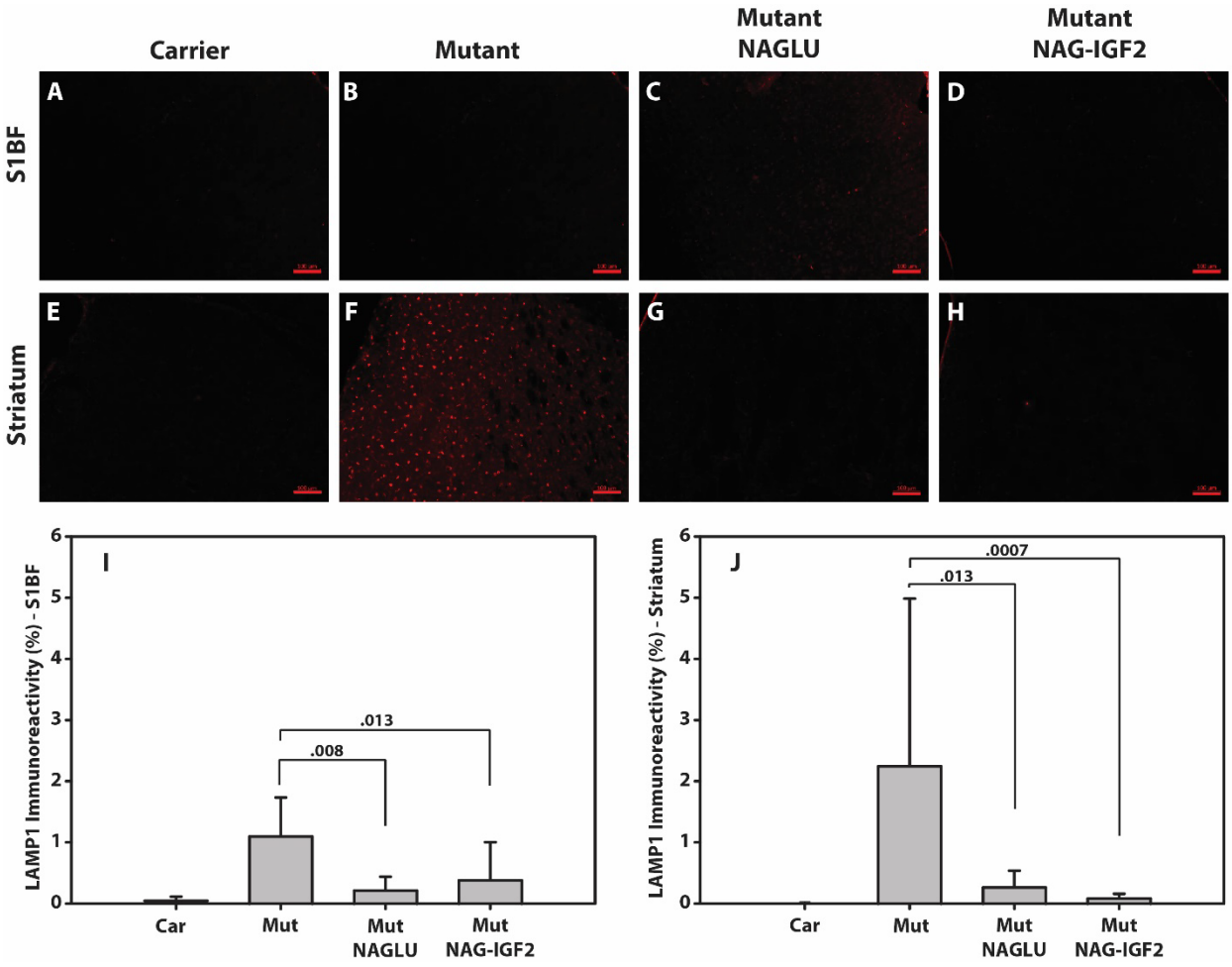

777

778 Figure 4

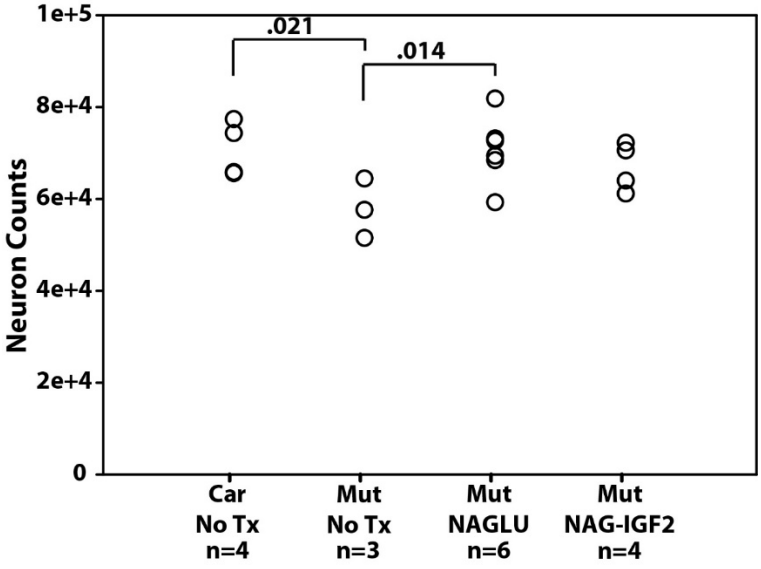

779

780 Figure 5

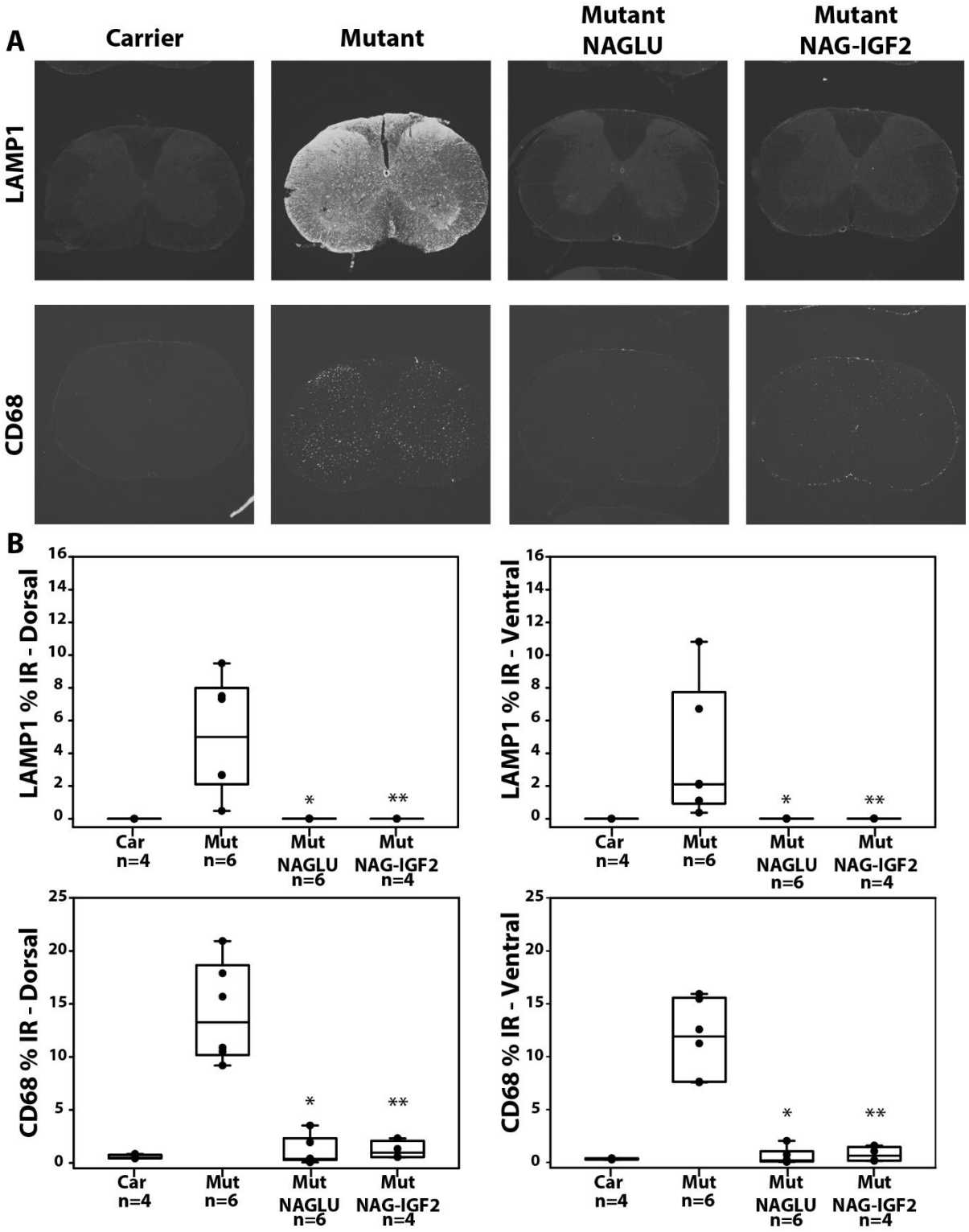

781

782 Figure 6

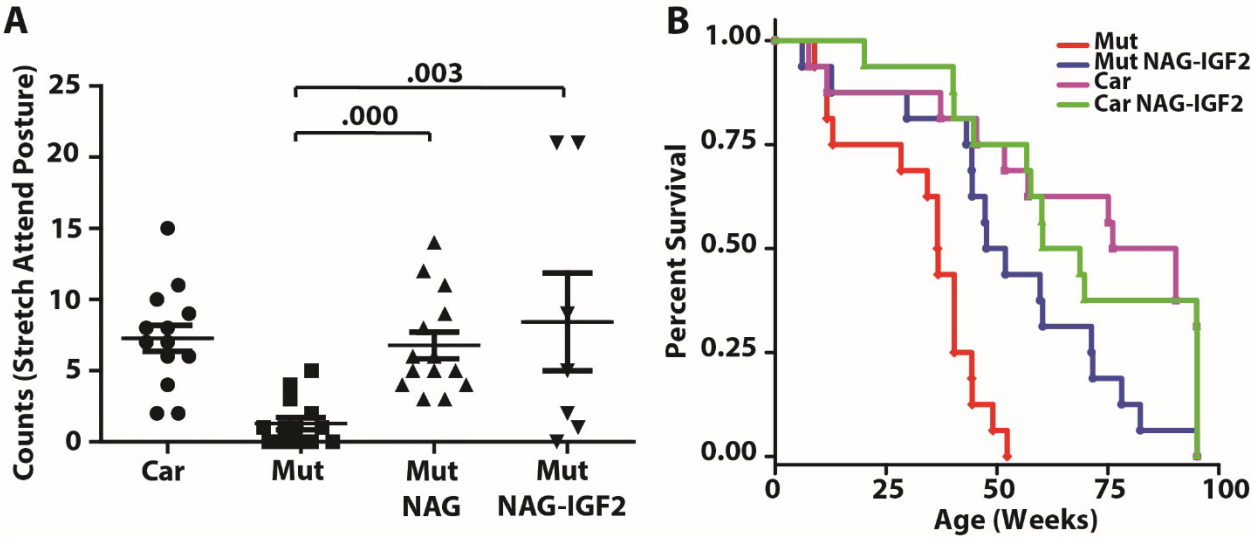

783

784 Figure 7

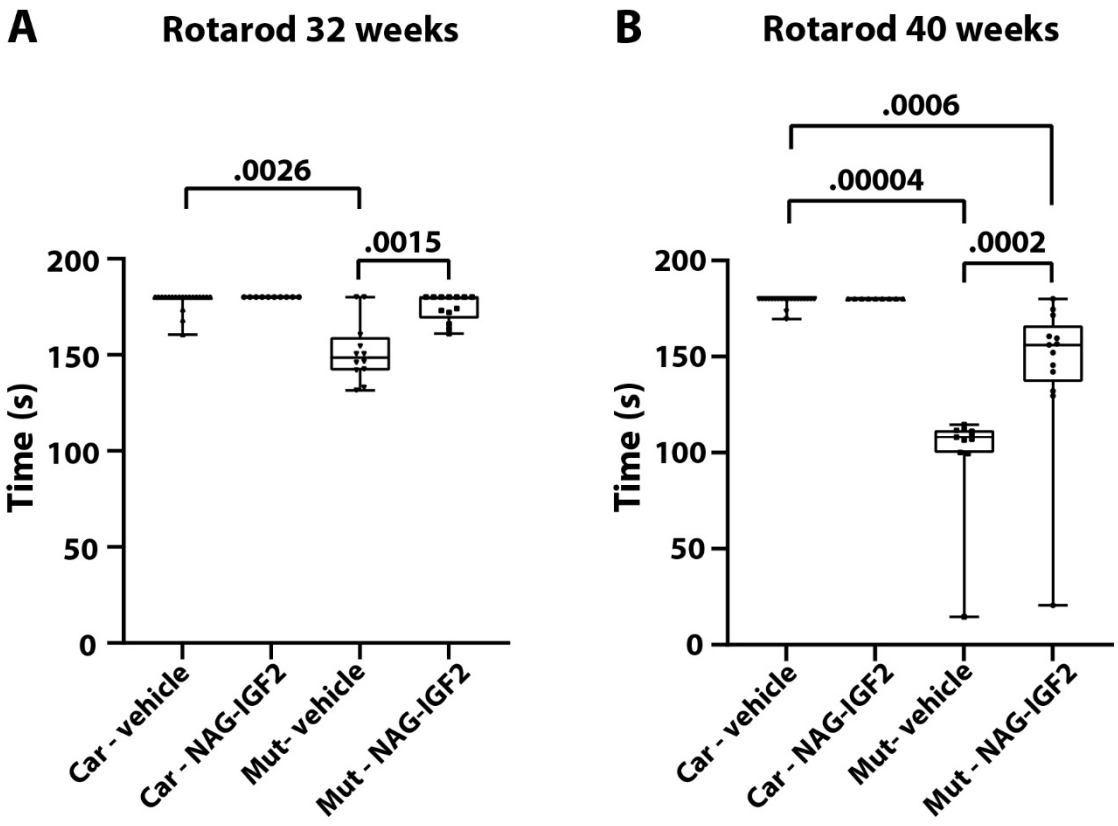

785

786 Figure 8

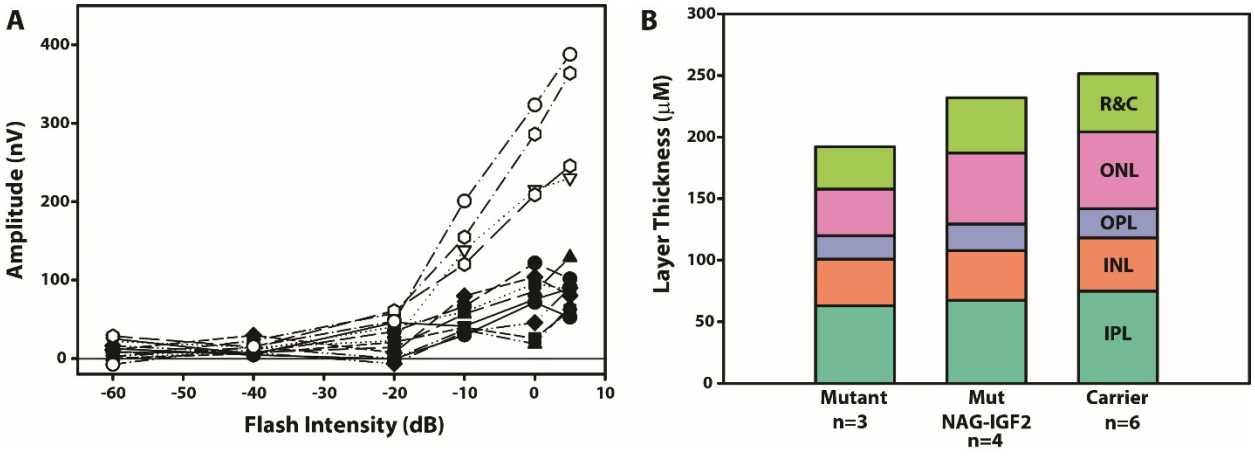

787

788 Figure 9

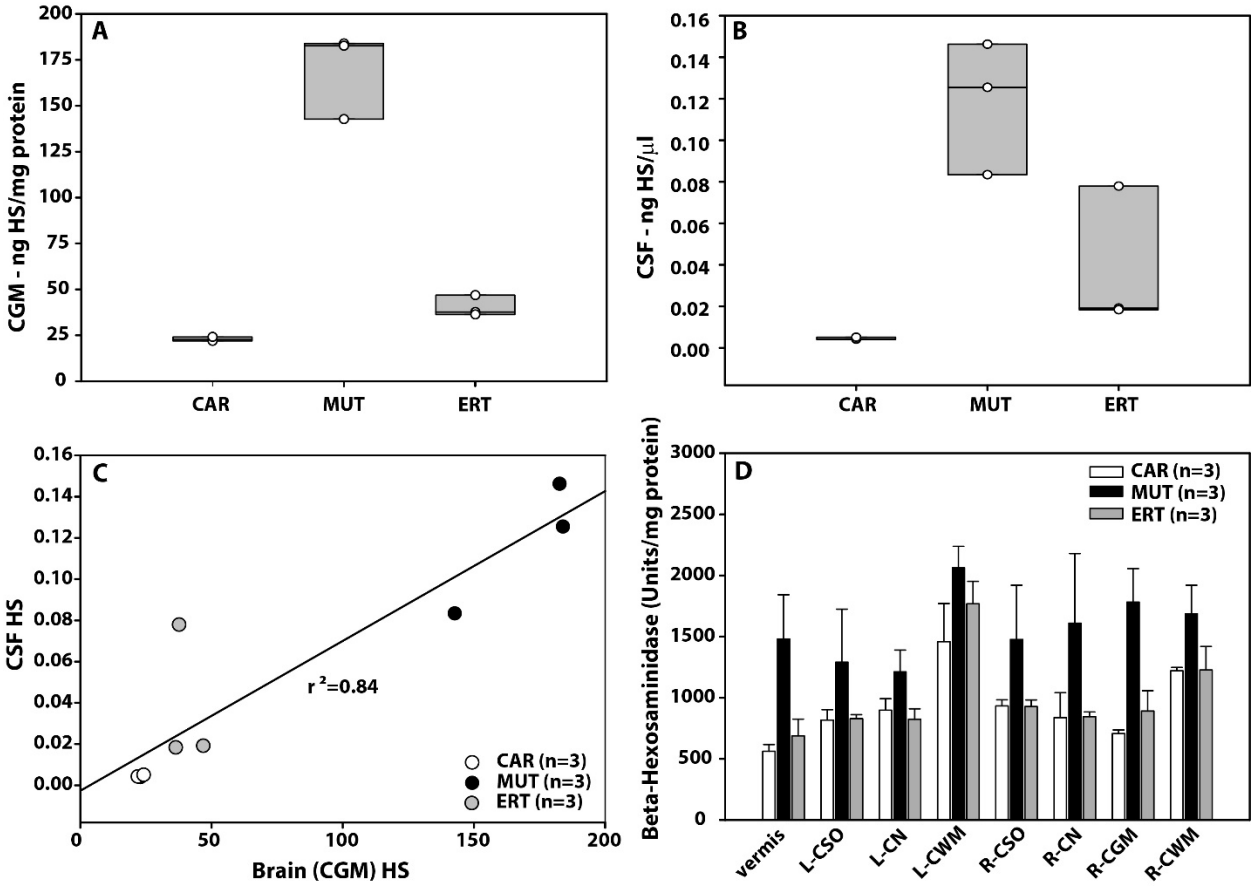

789

Figure 10

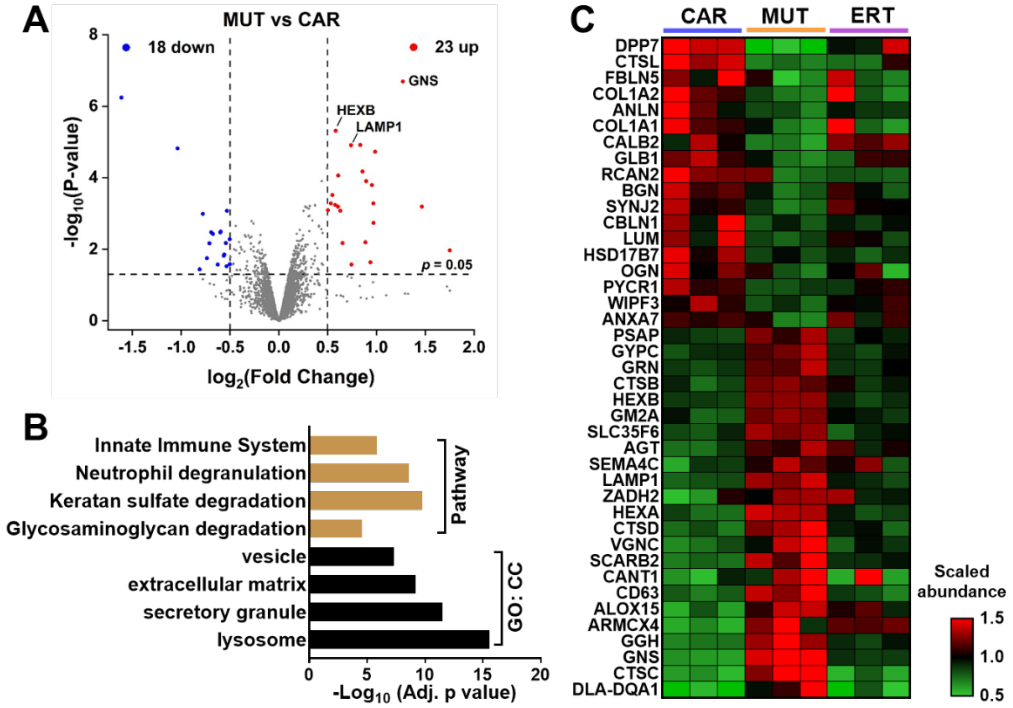
A
MUT vs CAR
18 down
23 up
GNS
HEXB
LAMP1
p = 0.05
-log10(P-value)
log2(Fold Change)
B
Innate Immune System
Neutrophil degranulation
Keratan sulfate degradation
Glycosaminoglycan degradation
Pathway
vesicle
extracellular matrix
secretory granule
lysosome
GO: CC
-Log10 (Adj. p value)
C
CAR
MUT
ERT
DPP7
CTSL
FBLN5
COL1A2
ANLN
COL1A1
CALB2
GLB1
RCAN2
BGN
SYNJ2
CBLN1
LUM
HSD17B7
OGN
PYCR1
WIPF3
ANXA7
PSAP
GYPC
GRN
CTSB
HEXB
GM2A
SLC35F6
AGT
SEMA4C
LAMP1
ZADH2
HEXA
CTSD
VGNC
SCARB2
CANT1
CD63
ALOX15
ARMCX4
GGH
GNS
CTSC
DLA-DQA1
Scaled abundance
1.5
1.0
0.5